

ENGN1735 Active Particles Technical Report
Sarah Nguyen, Helen Primis, Andrew Mombay, & Kaya Bruno
Mentor: Jack-William Barotta
Due: December 13, 2025
Project Name: HexCitations



Table of Contents

1. Introduction.....	3
2. Experimental Setup.....	4
3. Quantifying System.....	7
4. Model.....	8
5. Experimental Methods.....	11
6. Experimental Analysis and Model Comparison.....	11
7. Multifilament System.....	18
8. Conclusion.....	20
9. Appendix.....	22

Introduction

The background of our project lies within the study of active matter systems that are composed of active particles. An active particle moves autonomously by harnessing energy from its environment and converting it into self-propelled motion. Active matter systems are seen across nature, from the microscopic swarming of bacteria colonies¹ to the macroscopic motion of animal groups like schools of fish and flocks of birds.² Throughout these examples, active particles are inherently out-of-equilibrium, since each self-propelled particle breaks time-reversal symmetry. Therefore, active matter systems have the capability for complex collective behaviors to arise.¹ Examples of these behaviors include self-propelling locomotive functions, resource collection, local environmental restructuring, and particle aggregation.³

One topic of particular interest is the interplay of active systems that have elasticity. Such competing effects between activity and elasticity⁴ can lead to collective behavior such as synchronization.⁹ By investigating the relative strength of elastic forces to active forces, we gain insight into the driving force behind their collective motion. To this end, we aim to observe and analyze the collective synchronization behavior emergent upon coupling active particles with connectors of variable bendability.

Most studies of active motion feature microscopic particles⁵ or complex robotic systems, which require advanced technology and setup.⁶ To mitigate this, we propose using Hexbugs, small battery-powered toys, to serve as a macroscopic version of the often microscopic particles referenced in the relevant literature.⁷ Hexbugs have been used to probe the collective dynamics of other harder-to-measure systems given their centimetric size, steric, contact based interactions, and tunable properties such as propulsion speed.¹ Both variations in the surface on which the Hexbugs move, and the Hexbugs themselves cause them to change orientation, resulting in rotational diffusion and allowing a Hexbug in isolation to be modeled as an active particle subject to external noise. The Hexbugs generate momentum from their interaction with the surface under them, therefore serving as a representation of an active Brownian particle.¹

One particularly fruitful area in which Hexbugs have been used in recent research is in modeling biological systems.⁸ Considering applications of self-oscillations in active matter, biological systems at the microscopic level, such as cilia and flagella, are known to exhibit variable types of synchronous motion.⁹ Cilia are present on the surface of many cells, often

¹ Barona Balda, Angelo, Aykut Argun, Agnese Callegari, and Giovanni Volpe. "Playing with Active Matter." *The American Journal of Physics* 92 (November 2024): 847.

² Clemens Bechinger, Roberto Di Leonardo, Hartmut Löwen, Charles Reichhardt, Giorgio Volpe, and Giovanni Volpe. "Active particles in complex and crowded environments." *Review of Modern Physics* (November 2016): 1.

³ Sinaasappel, R., K.R. Prathyusha, Harry Tuazon, et al. Collecting Particles in Confined Spaces by Active Filamentous Matter. May 9, 2025, 1.

⁴ Ellen Zheng, Martin Brandenbourger, Louis Robinet, et al. "Self-Oscillation and Synchronization Transitions in Elastoactive Structures." *Physical Review Letters* (April 2023) 178202-1-2.

⁵ Q. Martinet, Y. I. Li, A. Aubret, E. Hannezo, and J. Palacci. "Emergent Dynamics of Active Elastic Microbeams." *Physical Review X* (October 2025): 1.

⁶ Alexey A. Dmitriev, Alina D. Rozenblit, Vadim A. Porvatov, et al. "Swarmodroid 1.0: A Modular Bristle-Bot Platform for Robotic Active Matter Studies." (May 2023): 1.

⁷ 3D Printable Hexbug Design and Instructions, [Blog Link](#).

⁸ Somnath Paramanick, Umashankar Pardhi, Harsh Soni, and Nitin Kumar1. "Spontaneous emergence of run-and-tumble-like dynamics in a robotic analog of Chlamydomonas: experiment and theory." (October 2025): 1.

⁹ Kirsty Wan. "Synchrony and symmetry-breaking in active flagellar coordination." *Phil. Trans. R. Soc. B* 375 (November 2019): 1.

taking the role of moving fluids in the body. By attaching multiple Hexbugs in line through elastic linkages, we model a filament similar to a cilium.¹⁰

Moreover, relevant literature investigates the behaviors of various configurations of cilia-like appendages when attached to a central body. Studies have examined two-legged gaits in which two filaments are attached to the central body. We look to investigate four-legged gaits, representative of quadriflagellates (four-armed apparatuses).⁸ By attaching multiple of these Hexbug filaments to a center pin, this macroscopic experiment can help to model the collective motion seen in microscopic biological phenomena.

In order to accomplish this investigation into Hexbugs as active particles, we begin with an experimental setup detailing the components used to link and track the Hexbugs, followed by quantifying the experimental system through numerical parameters. We also introduce the mathematical model governing the experiment and compare the experimental data to that of the model. Lastly, we qualitatively investigate multifilament systems, specifically two and four-armed apparatuses.

Experimental Setup

The experimental setup for this project consists of three main components to create Hexbug filaments. The first is the Hexbug itself, which are macroscopic representations of Brownian particles (*Figure 1a*). The second is a 3D-printed cage (PLA filament and BambuLabs A1 with an infill of 15%) that attaches to the body of the Hexbug. This cage provides a connection point between multiple Hexbugs and features a tracking ArUco code generated by MATLAB or Python scripts as provided in the repository (*Figure 1b and 1c*). The ArUco codes would eventually aid in our tracking endeavors through Python later on. The third is a silicone rubber linkage made from a two-part liquid silicone rubber compound that serves to join multiple Hexbugs together (*Figure 2*). Our experiment consisted of attaching the Hexbugs with linkages of four different lengths, all with the same cross sectional area. By design, the keyhole style linkages attach the Hexbug cages to each other, and the first Hexbug to a central body while ensuring that the linkage will only bend and prevent rotation.

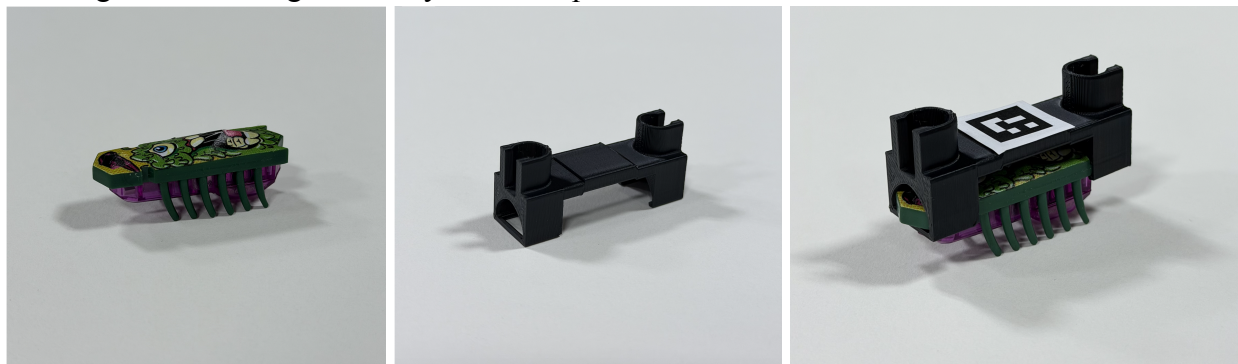


Figure 1: (a) Singular Hexbug, (b) 3D Printed Hexbug Cage, (c) Hexbug Mounted with Cage and ArUco tracking code

¹⁰ Yiming Xia, Zixan Hu, Da Wei, Ke Chen, Yi Peng, and Mingcheng Yang. “Biomimetic Synchronization in Biciliated Robots.” *Physical Review Letters* 133, 048302 (July 2024): 048302-1.

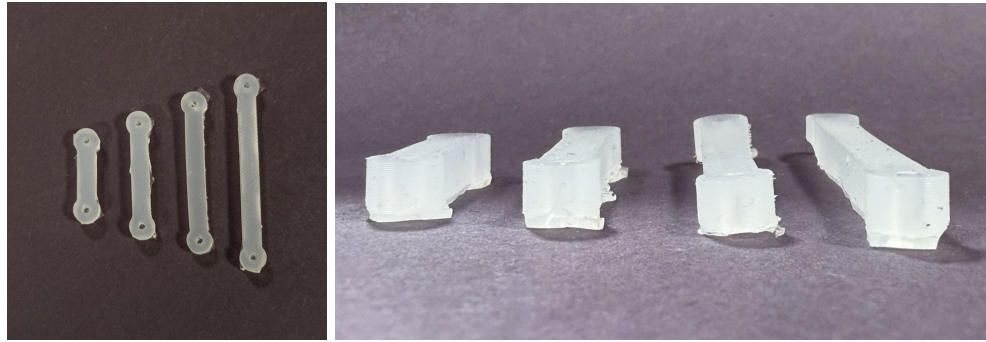


Figure 2: (a) Silicone Linkages Plane View, (b) Silicone Linkages Cross Sectional View

Initial experiments focused on singular filament behavior, including three or four Hexbugs connected with silicone linkages of various lengths to a central, rectangular, base that inhibited rotation of the linkage (*Figure 3*). Collective Hexbug behavior is dictated by three main factors: the active force of each bug, the drag force, and the bending capability of the link (which we later will describe through a dimensionless constant, σ). The active force is set by the manufacturer when using commercially available Hexbugs; since battery replacements are possible, the active force of each bug can be slightly adjusted as batteries need to be replaced. The drag force is dictated by the surface on which the testing takes place; for consistency, all of our testing was conducted on a matte finish, thin, rigid plastic sheet with moderate friction. By testing on different surfaces (printer paper, construction paper, wooden tables), we found that the plastic provided us with little enough friction for movement to occur for filaments with only a few Hexbugs, and enough friction for the system to oscillate slowly enough for us to track movement and angles. The bending capability associated with each linkage was dictated by our design choices and material selection. Through various iterations, we found that a 5 mm x 5 mm cross-section was an appropriate size for utilizing 3D-printed molds to shape the rubber while not coming out too stiff after curing for 18 hours. We varied the length of each linkage to produce various bending motions, corresponding dimensionless numbers, and constants as outlined in later sections. In turn, considering the active force and the drag force as constants of the system, Hexbug behaviors were primarily dependent on the bending behavior of the linkages as we changed them for each trial.

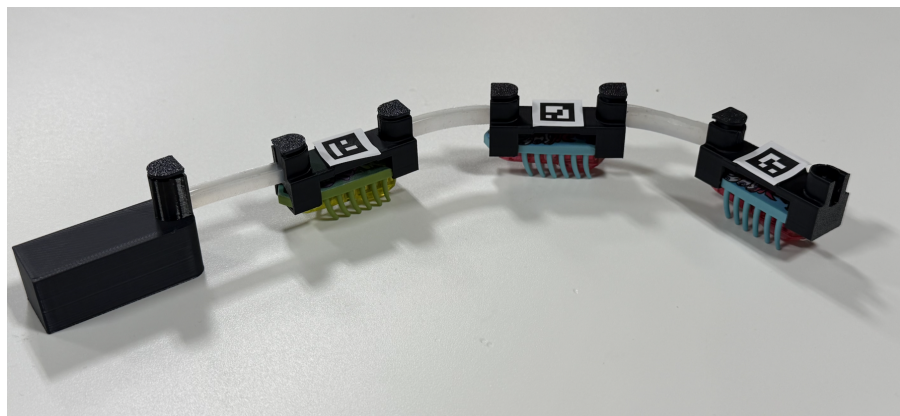


Figure 3: Hexbug Filament with Three Hexbugs

After concluding the testing of a single filament system with different linkages, further experimental setups included multiple filament systems connected to a central body, as seen below with two and four filaments attached (*Figures 4a and 4b*). We will qualitatively explore the two filament and four filament systems later on in the Multifilament section when attached to a stationary central body and a rotating central body.

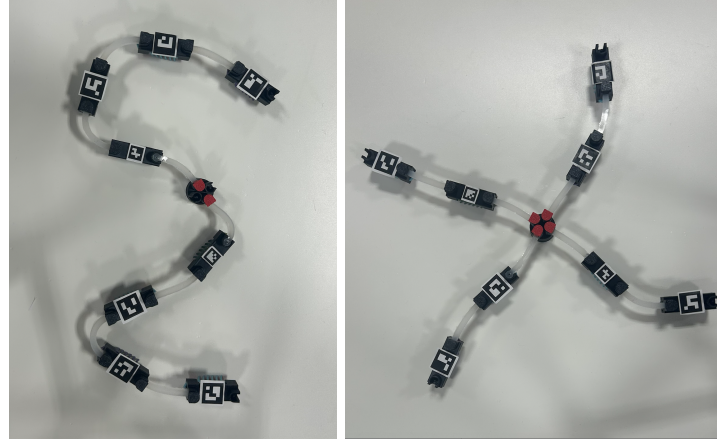


Figure 4: (a) Two Hexbug Filaments Connected to Central Body, (b) Four Hexbug Filaments Connected to Central Body

In order to record our findings, we used a tripod (courtesy of the Harris Lab) and an iPhone shooting at 120 frames per second. *Figure 5* shows the tripod and phone in relation to the filament. We outline our data processing and resulting graphs in the following sections.



Figure 5: N = 3 Hexbug system trial set up with tripod and phone camera.

Quantifying System

To analyze the experiment we define the following parameters below and the method or equation used to obtain each parameter.

1. Spring Constant (k): determined for each linkage length by hanging known masses (m) from the linkages and using MATLAB image processing to calculate keyhole to keyhole displacement (x)

$$k = \frac{F}{x} \text{ where } F = mg$$

2. Young's Modulus (E): determined for each linkage length with the following equation where L = linkage length from keyhole to keyhole and A = linkage cross sectional area

$$E = \frac{FL}{Ax}$$

3. Torsion Constant (J): the same value for each linkage length, determined with the following equation where a = 2.5 mm (half of the height of the linkage) and b = 2.5mm (half of the width of the linkage)

$$J = ab^3 \left(\frac{16}{3} - 3.36 \frac{b}{a} \left(1 - \frac{b^4}{12a^4} \right) \right) = 88.0208 \text{ mm}^4 \text{ }^{11}$$

4. Torsional Stiffness (C): determined for each linkage length with the following equation

$$C = \frac{EJ}{L}$$

5. Elastoactive Parameter (σ): from supplementary material, the elastoactive parameter is a dimensionless group that represents the ratio between the active force of the Hexbug to bending force intrinsic to the rubber linkages. Therefore, for small values of σ , straight line trajectory is expected. For sigma values above a critical elastoactive parameter (σ_c) that depends on the number of bugs in a chain, limit cycle trajectory is expected with large oscillatory bending behaviors. l in the equation below is defined as the total end-to-end length of the rubber linkage instead of just the keyhole to keyhole length (L), as mentioned before when calculating the material properties. In turn, σ was determined for each linkage length with the following equation

$$\sigma = \frac{F_a l}{C} \text{ where } F_a = 15.7 \pm 3.1 \text{ mN (average force of pinned Hexbug)} \text{ }^{11}$$

6. Characteristic Timescale (τ): from supplementary material, the characteristic timescale results from a ratio of drag force per Hexbug to the stiffness of each linkage. The isotropic viscosity (ψ) acts as a damping force calculated by the ratio of the active force to the average velocity of a freely moving Hexbug, and l is the length of the pendulum as defined above for σ .

$$\tau = \frac{\psi l^2}{C} \text{ where } \psi = 0.63 \pm 0.11 \text{ Ns/m (isotropic viscosity)} \text{ }^{11}$$

While τ is used in the energy derivation for our system in the following section, this timescale plays a minimal role in dictating the onset of collective behavior of the Hexbugs. τ sets the frequency of self-oscillation, but does not dictate the onset of oscillation. σ , on the other hand, entirely determines the ability for a system of N Hexbugs to oscillate and at what magnitude.

¹¹ Ellen Zheng, et al. "Self-oscillation and Synchronisation Transitions in Elasto-Active Structures: Supplementary Information." Physical Review Letters (April 2023) 3.

With these parameters defined, the values for various linkage lengths are reported in the table below. The cross section, held constant across all four lengths, is a 5 x 5 mm square. These values were determined utilizing a series of MATLAB code that can be found in the repository.

Length l (mm)	27.3	37.3	47.3	57.3
Spring constant k (N/mm)	.2152	0.1266	0.1094	0.1001
Averaged Axial Young's Modulus E (MPa)	0.132			
Torsional Stiffness C (Nm/rad)	9.45e-4	5.21e-4	3.60e-4	2.75e-4
Elastoactive Parameter σ	1.0071	1.8800	3.0232	4.4366
Characteristic Timescale τ (s)	1.1032	2.8139	5.7381	10.2011

Table 1: Parameters for linkage lengths 1-4.

A prior paper we explored noted that σ values between 0.05 and 3 demonstrated collective behavior when at least $N = 2$ bugs were attached for the higher sigma values and as many as $N = 9$ bugs connected for the smallest σ values.¹ Since σ has a linear dependency on the length of the linkage, our σ values increase as our length increases. The array of four different σ values between 1.0071 and 4.4366 will enable us to explore the critical N for oscillation with smaller values, and how the oscillation will evolve as we progressively increase the magnitude of this parameter.

Model

Our model utilizes Hexbugs as macroscopic Brownian particles and silicone rubber to link from one component to the next, similar to the 2023 Zheng paper as referenced. In modeling our system, we have ignored both the inertia of an individual bug and noise. It has been shown previously that both effects are secondary to the active and bending forces that dictate the filament's behavior. The math utilized in our tracking and simulation code is outlined here, with modifications to inconsistencies from the Zheng paper. A figure for reference (*Figure 6*) is provided to illustrate variables referenced in this section.

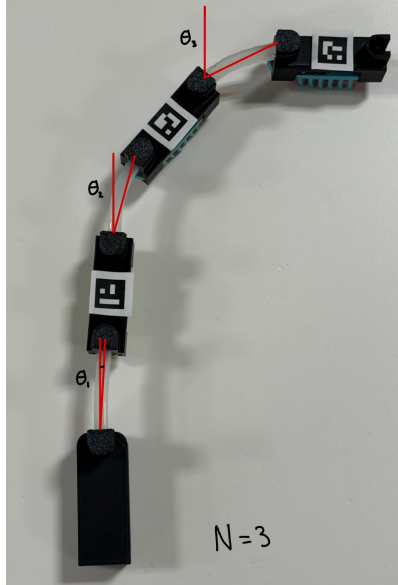


Figure 6: Labeled $N = 3$ filament systems describing angles as they appear in the energy balance below.

The single filament with N -components is connected to a stationary wall and linked through beams of torsional stiffness C such that a high C corresponds to a stiff linkage and a low C corresponds to a more flimsy linkage. The potential energy of our system, U , can be discretized into a summation relating the relative bending angle of each linkage and the torsional constant:

$$U = \frac{c}{2} \theta_1^2 + \frac{c}{2} (\theta_2 - \theta_1)^2 + \frac{c}{2} (\theta_3 - \theta_2)^2 + \dots$$

This can be re-written into the following summation:

$$U = \frac{c}{2} \theta_1^2 + \sum_{i=2}^N (\theta_i - \theta_{i-1})^2$$

where the first term with θ_1 is the potential energy from the wall to the first component and the summation is the potential energy relative between each bug and its neighbor.

In this system, there are two main forces at play: active forces (which we will define in terms of bending and the associated constant σ later) and drag forces. For each particle driven by their individual motor, their active force can be written as:

$$\bar{F}_{A,i} = F_a (-\cos\theta_i \hat{i}, \sin\theta_i \hat{j})$$

In regards to the the drag force, these types of forces are isotropic, linearly dependent on the friction coefficient, μ , and linearly dependent on velocity:

$$\bar{F}_{D,i} = -\mu(\dot{x}_i - \dot{y}_i)$$

Now, we can relate our net force from the active forces and drag forces to potential energy through the Virtual-Work Theorem at equilibrium:

$$\delta W = \delta U \rightarrow 0 = \delta U - \delta W$$

where δW is the variation of work from the forces and δU is the variation of potential energy. Using the energy balance instead of the force balance enables us to capture the highly coupled

system we are working with in one summation. Expanding out δW in terms of force summations and using a displacement of $\delta d = \delta \hat{x} + \delta \hat{y}$, we get:

$$\delta W = \delta(Fd) = d(\sum F_D - \sum F_A) = -\mu \sum_{i=1}^N (\dot{x}_i \delta x_i + \dot{y}_i \delta y_i) - F_A \sum_{i=1}^N (\cos \theta_i \delta x_i + \sin \theta_i \delta y_i)$$

To expand out the potential energy using $\delta \theta_i$ for the change in angle between each component, we get:

$$\delta U = C(2\theta_1 - \theta_2)\delta \theta_1 + C(2\theta_2 - \theta_3)\delta \theta_2 + \dots$$

Employing trigonometric relationships between θ_i and x_i and the length of the linkage l , we will be able to write δW entirely in terms of θ_i and $\delta \theta_i$:

$$x_i = \sum_{i=1}^N l \cos \theta_i \text{ and } y_i = \sum_{i=1}^N l \sin \theta_i$$

Now substituting in to the work summation:

$$\delta W = -\mu l^2 \sum_{i=1}^N \sum_{j=1}^i \sum_{k=1}^i (\cos(\theta_j - \theta_k) \dot{\theta}_j \delta \theta_k) - F_A l \sum_{i=1}^N \sum_{j=1}^i (\sin(\theta_i - \theta_j) \delta \theta_j)$$

These summations will enable us to find two non-dimensional constants, σ and τ , that will streamline our work-energy balance to be a solvable linear system through computation. We will define σ , the elastoactive dimensionless parameter as the relationship between activity and stiffness:

$$\sigma = \frac{\text{Activity}}{\text{Stiffness}} = \frac{F_A l}{C}, \sigma \sim \frac{\text{Activity}}{\text{Elasticity}}$$

If σ is low, we will see minimal self-oscillation and bending. If σ is large, we will see lots of movement and self-oscillation. With our linkage design, we held the cross-sectional area constant and varied the length of the link; in turn, as our linkages increased in length, their sigma values also increased in magnitude.

We will define τ as the timescale resulting from a balance of drag and stiffness:

$$\tau = \frac{\text{Drag}}{\text{Stiffness}} = \frac{\varphi l^2}{C}, \tau \sim \frac{\text{Drag}}{\text{Elasticity}}$$

With a higher τ , we will see a slower movement and oscillation; with a lower τ , we will see more rapid oscillations. Now subbing our dimensionless numbers into our energy balance to get energy expressions for Bug 1, Bugs 2-N-1, and Bug N:

$$\text{For Bug 1: } 0 = 2\theta_1 - \theta_2 - \sigma \sum_{j=i}^N \sin(\theta_1 - \theta_j) + \tau(N\dot{\theta}_i + \sum_{j=2}^N (N-j+1)\dot{\theta}_j \cos(\theta_j - \theta_i))$$

$$\text{For Bug 2 - Bug N - 1: } 0 = 2\theta_i - \theta_{i+1} - \theta_{i-1} - \sigma \sum_{j=i}^N \sin(\theta_i - \theta_j) +$$

$$\tau[(N-i+1) \sum_{j=1}^i \dot{\theta}_j \cos(\theta_i - \theta_j) + \sum_{j=i+1}^N (N-j+1) \dot{\theta}_j \cos(\theta_j - \theta_i)]$$

$$\text{For Bug N: } 0 = \theta_N - \theta_{N-1} + \tau \sum_{j=1}^N \dot{\theta}_j \cos(\theta_N - \theta_j)$$

Using the three equations above that characterize Bug 1, Bug 2 through Bug N-1, and Bug N, we are able to create a set of differential algebraic equations that can be solved in MATLAB using readily available solvers such as ODE45 to solve for the time derivative of the angle.

Experimental Methods

For all of our trials, 30-40 second videos (3600-4800 frames) were taken with an iPhone mounted on a tripod so that any notable oscillation went through multiple, stable periods. This aided our digital processing, smoothing out the data with many sets of data points across the same path. For the sake of presenting the oscillation in the following section, four photos were taken throughout one period of oscillation to illustrate the motion: the left-hand maximum, crossing the centerline from the left to right, right-hand maximum, and crossing the centerline from the right to left. These snapshots will be compared to our simulation developed graphs as well.

The first trial began with linking $N = 3$ Hexbugs together with the 27.3 mm linkage and attaching to a central body attached to the surface. The second trial linked $N = 4$ Hexbugs and the same linkage length of 27.3 mm. The third, fourth, and fifth trials consisted of connecting $N = 3$ Hexbugs with the 37.3 mm, 47.3 mm, and 57.3 mm linkages respectively, with each filament connected to the same stationary base. In the following section, we will explore our experimental video results and the live Python tracking performed for each of our five trials. Then, we will compare our findings to the mathematical model outlined above and computed by MATLAB.

Experiment Analysis and Model Comparison

We began our analysis with visual inspection of the experimental trials by comparing the Hexbug to its counterpart simulation at four specific points in its oscillation (when applicable). From these images of our own experiments juxtaposed to the simulation's predictions, we are able to compare qualitatively and observe the fit of our own experiments with the governing model. In addition, to compare the experimental videos and the model, we plotted three graphs. The first is the x-y position which shows the trajectory of the Hexbug filament. The second is mean curvature versus time. Mean curvature is the angle of the first Hexbug minus the angle of the last Hexbug in the chain. As a note, for all of our experimental curvature graphs compared to simulation graphs below, we saw much more frequent oscillation in real life than in the simulation; the shape of the curvature, however, was practically identical. The third graph shows the mean polarization versus mean curvature, with the mean polarization being the average angle of all Hexbugs. This represents the phase space, in which more oscillation leads to a more elliptic phase space and no oscillation results in a dot. In turn, we saw more of an elliptic output from our higher σ values.

Trial #1 is shown in *Figure 7* with $\sigma = 1.0071$ and $N = 3$ Hexbugs. We observed a similar response between the two with no visual oscillation taking place. When comparing the trajectory, mean curvature vs. time, and phase space plots, as shown in *Figure 8* between the experimental vs. simulation, we saw no visual oscillation take place in both the model and the experiment. Importantly, the phase plot had no visible elliptic nature or pattern to it, as our prediction suspected for a low σ filament.

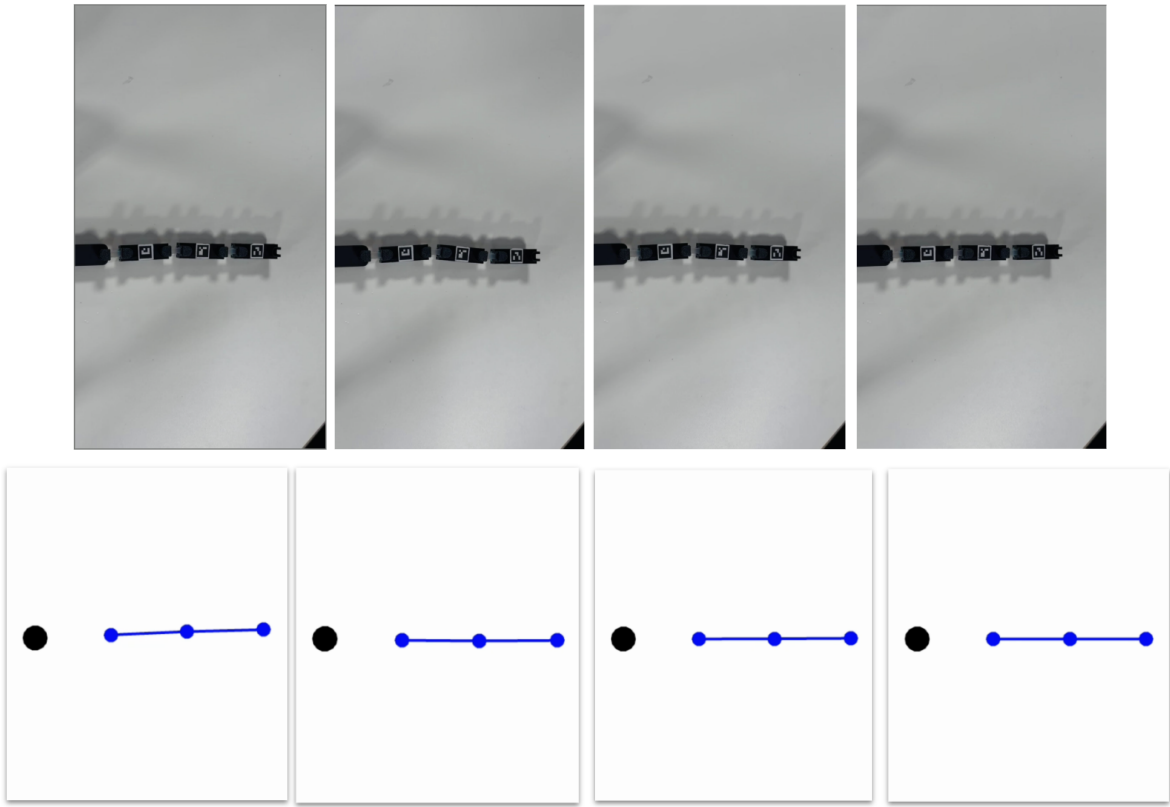


Figure 7: Trial #1 ($N = 3, \sigma = 1.0071$) Experimental reference frames (top row) and Simulation reference frames (bottom row)

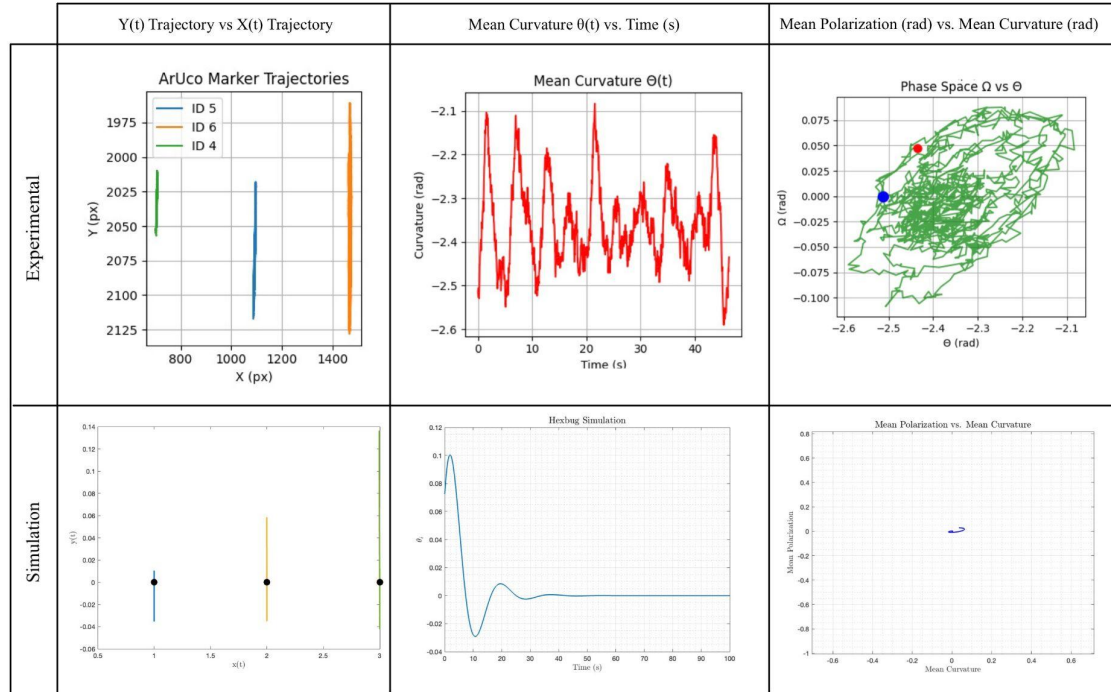


Figure 8: Trial #1 Graphs ($N = 3, \sigma = 1.0071$) Experimental Tracking data and corresponding graphs (top row) and Simulation generated graphs (bottom row)

With Trial #2 shown in *Figure 9* with $\sigma = 1.0071$, $N = 4$ Hexbugs, we importantly saw oscillation even though we were using the same linkages as Trial #1; thus, we discovered that the onset of oscillation is dependent on both N number of Hexbugs and the σ value for the linkage. Additionally, we saw similar responses to those of our simulation. There were minor discrepancies observed between our experimental snapshots and the animation, which is expected due to real-life testing conditions compared to the simulation. In *Figure 10*, we see a strong correlation between our tracking data compared to that of the simulation, including a more elliptic phase response since we saw oscillation in this test.

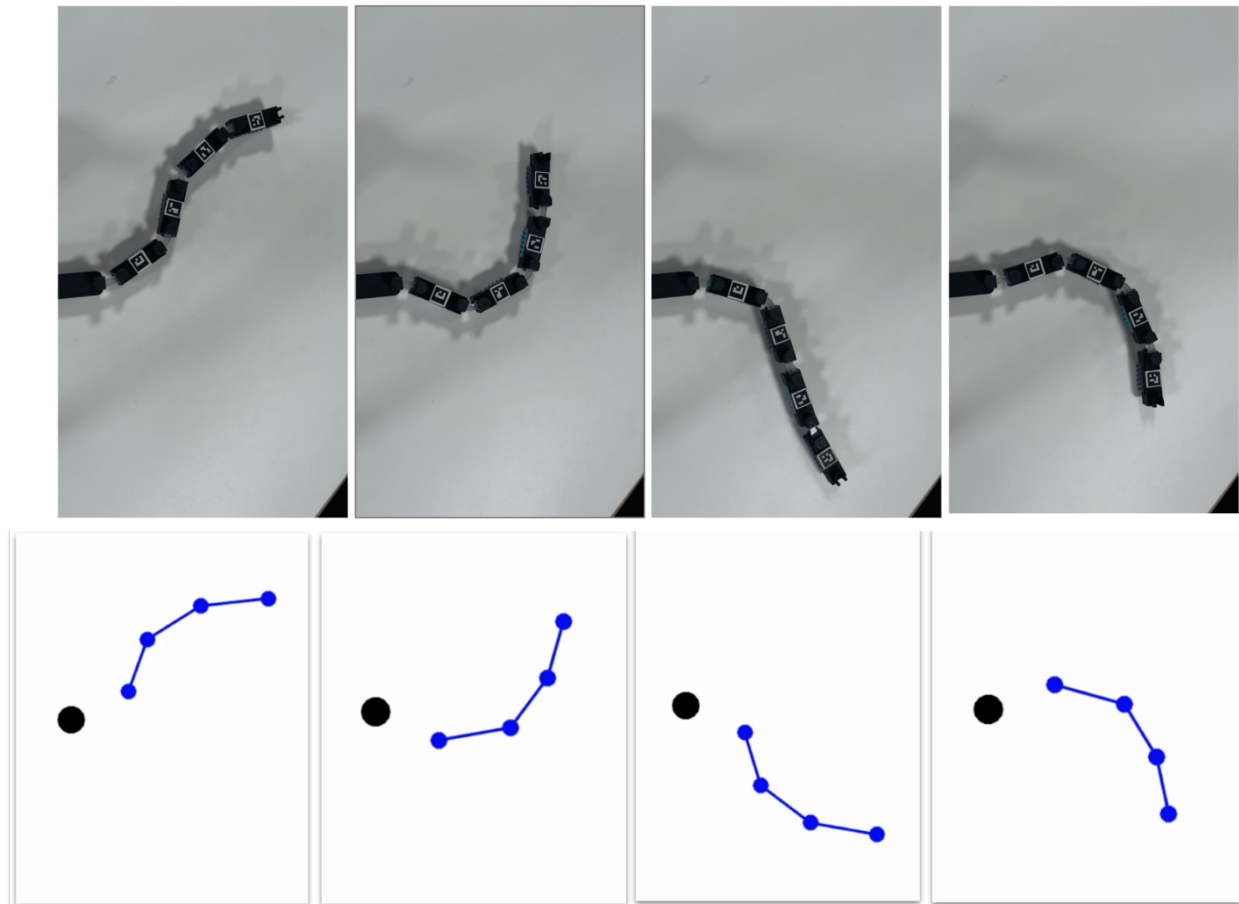


Figure 9: Trial #2 ($N = 4$, $\sigma = 1.0071$) Experimental reference frames (top row) and Simulation reference frames (bottom row)

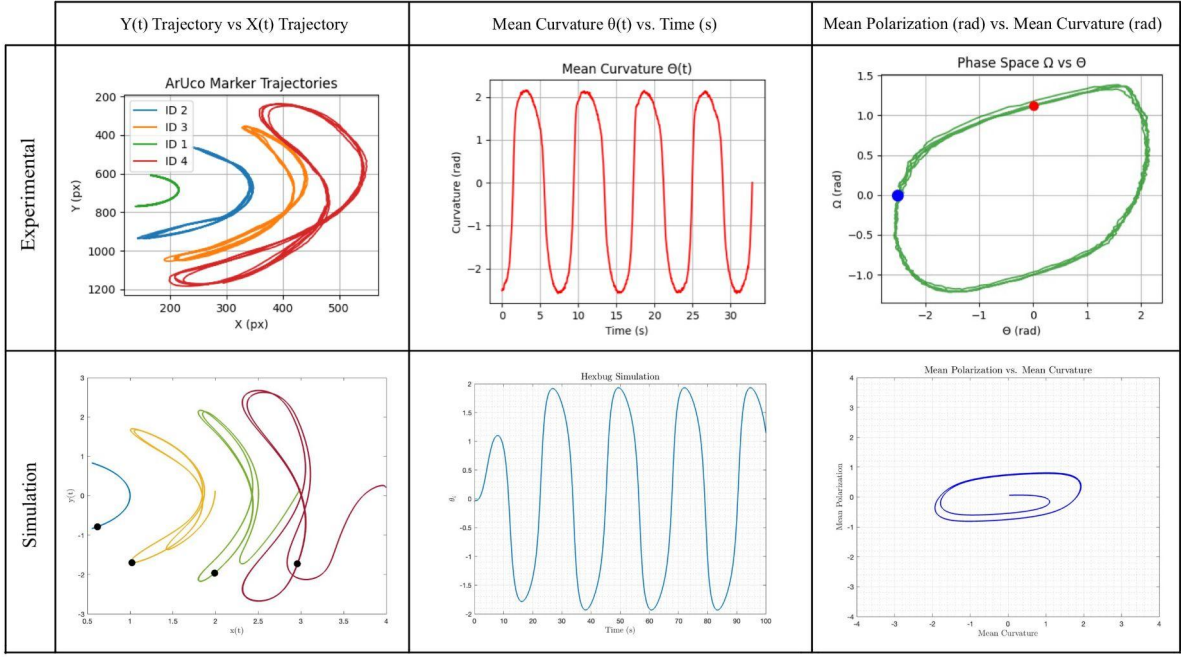


Figure 10: Graphs for Trial #2 ($N = 4$, $\sigma = 1.0071$) Tracking data and corresponding graphs (top row) and Simulation generated plots (bottom row)

Trial #3, as seen in *Figure 11*, with $\sigma = 1.8800$, $N = 3$ Hexbugs, we see clear oscillation; thus, we know that $N = 3$ is above the critical number for this σ to have oscillations. Comparing the simulation to our experiment, we can see the similarities in movement between the real and simulated three Hexbug systems. Examining the tracking data from the experiments versus the simulation data in *Figure 12*, we see that our two sets of graphs generally agree, proving the viability of our simulation for a σ of this magnitude. Taking a deeper dive, we identify that the amplitude of the mean curvature in our experiment and our simulation is in agreement, while we do have some discrepancies in the mean polarization, which can be due to the magnitude of movement of the Hexbugs being larger in the experiment than in the simulation.

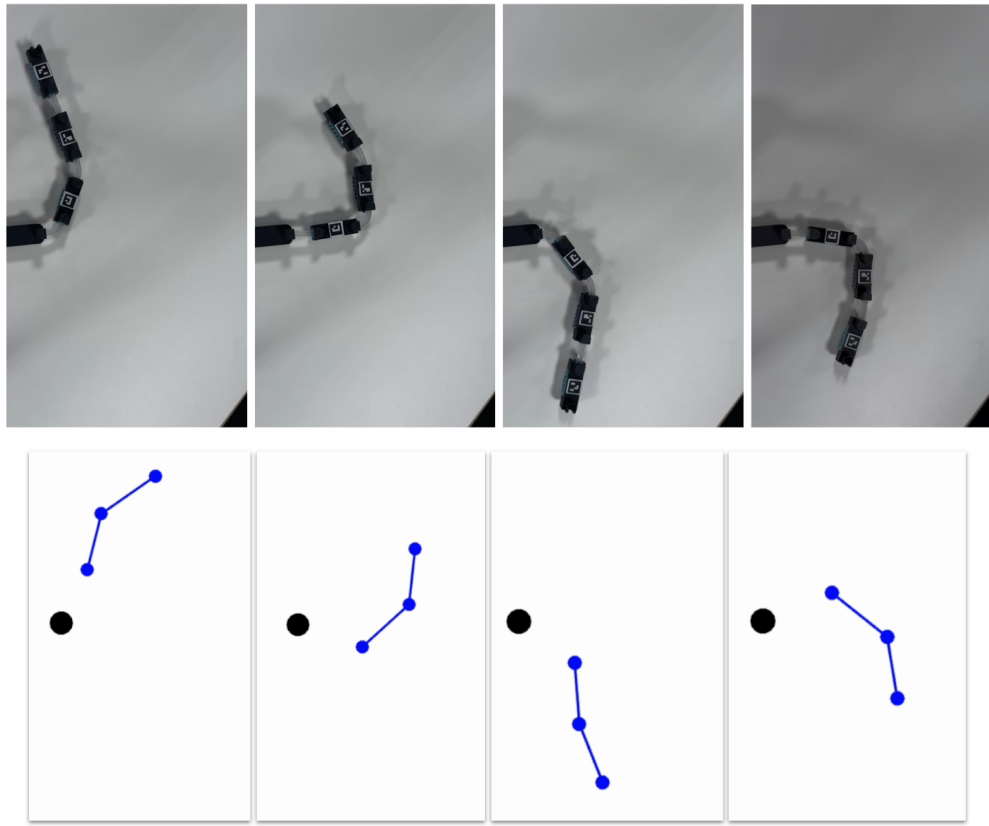


Figure 11: Trial #3 ($N = 3, \sigma = 1.8800$) Experimental reference frames (top row) and Simulation reference frames (bottom row)

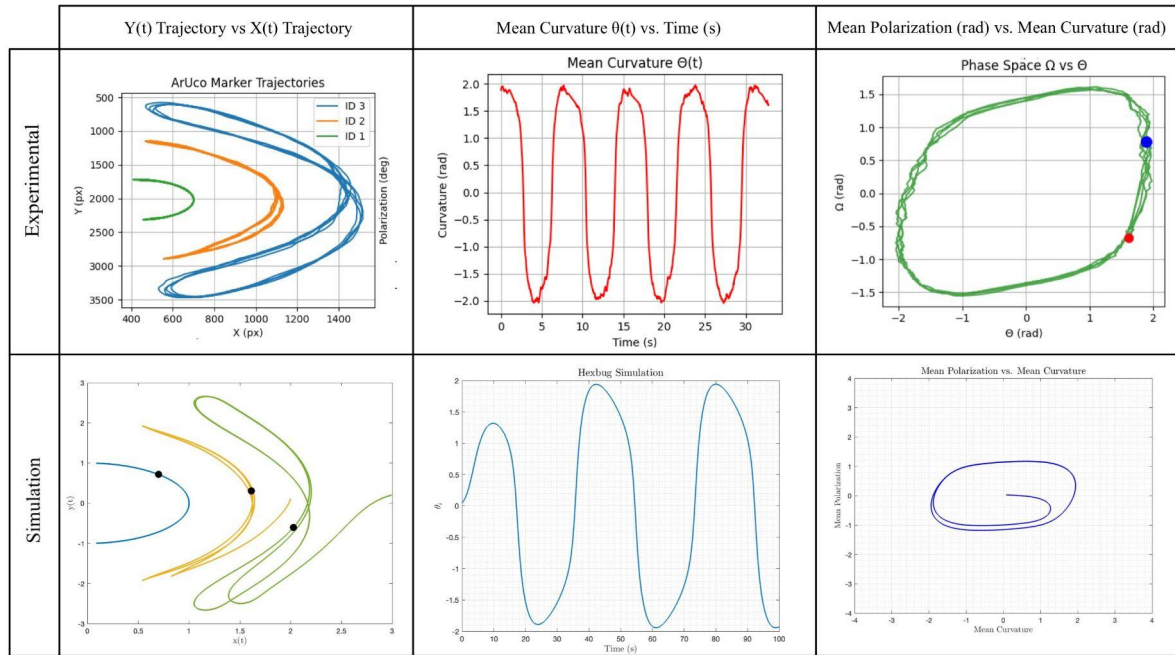


Figure 12: Trial #3 ($N = 3, \sigma = 1.8800$) Tracking data and corresponding graphs (top row) and Simulation generated plots (bottom row)

Next, taking a look at Trial #4, we are still continuing to ratchet up the length of our linkages. This trial included linkages of $\sigma = 3.0232$ and $N = 3$ bugs which resulted in larger oscillations than observed in the previous three trials. One major difference between our experimental snapshots and experimental snapshots is that the simulation moves significantly past the zero line of our central body while the real life experiment does not (*Figure 13*). This discrepancy can be attributed to the facts that our keyhole design government our cages and linkages does not permit for such dramatic bending of the first bug; the simulation is idealized to not take this type of real-world constraint into account, and only focuses on the increased σ value increasing the magnitude of the path. In *Figure 14*, the discrepancies between our tracking and the simulation graphs corresponds to the difference in magnitude we see in *Figure 13*. Overall, the shape resemblance between our path and angle measurements mirror those found in the simulation – a commonality seen in all trials before this as well.

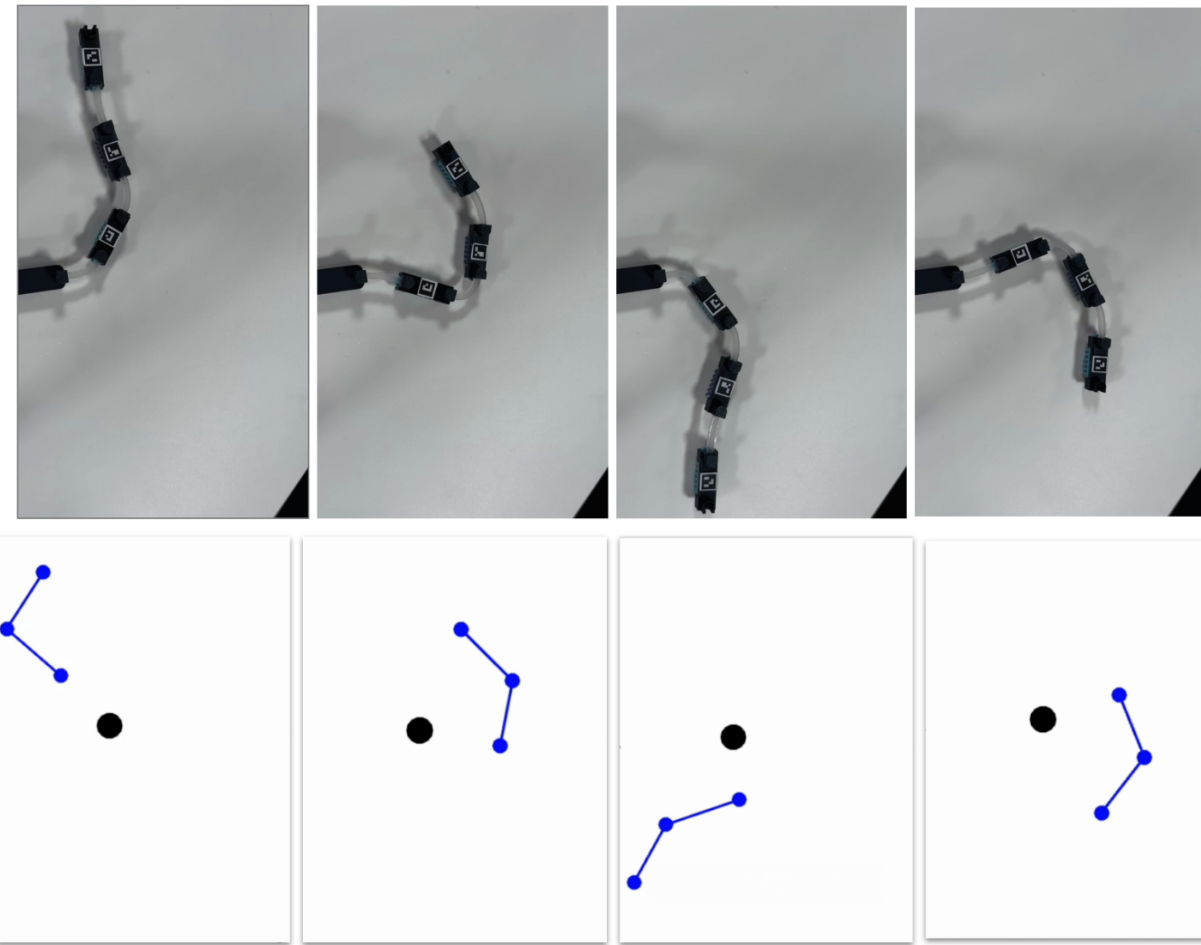


Figure 13: Trial #4 ($N = 3, \sigma = 3.0232$) Experimental reference frames (top row) and Simulation reference frames (bottom row)

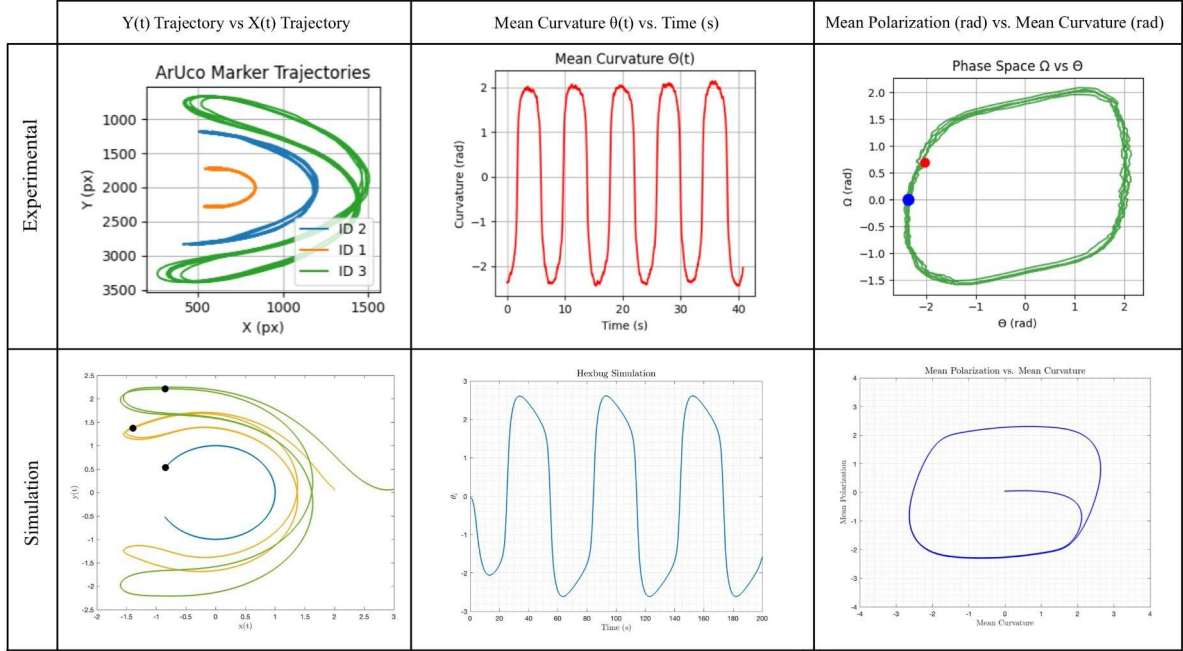


Figure 14: Trial #4 ($N = 3, \sigma = 3.0232$) Tracking data and corresponding graphs (top row) and Simulation generated plots (bottom row)

Lastly for Trial #5, as shown in *Figure 15* with $\sigma = 4.4366$, $N = 3$ Hexbugs, we see a discrepancy between the experimental and simulation. The simulation goes further beyond the zero line, similar to Trial #4. Furthermore, considering the graphs shown in *Figure 16*, we see a general agreement between the experimental and simulated trajectories with the magnitude difference playing a role in the variation.

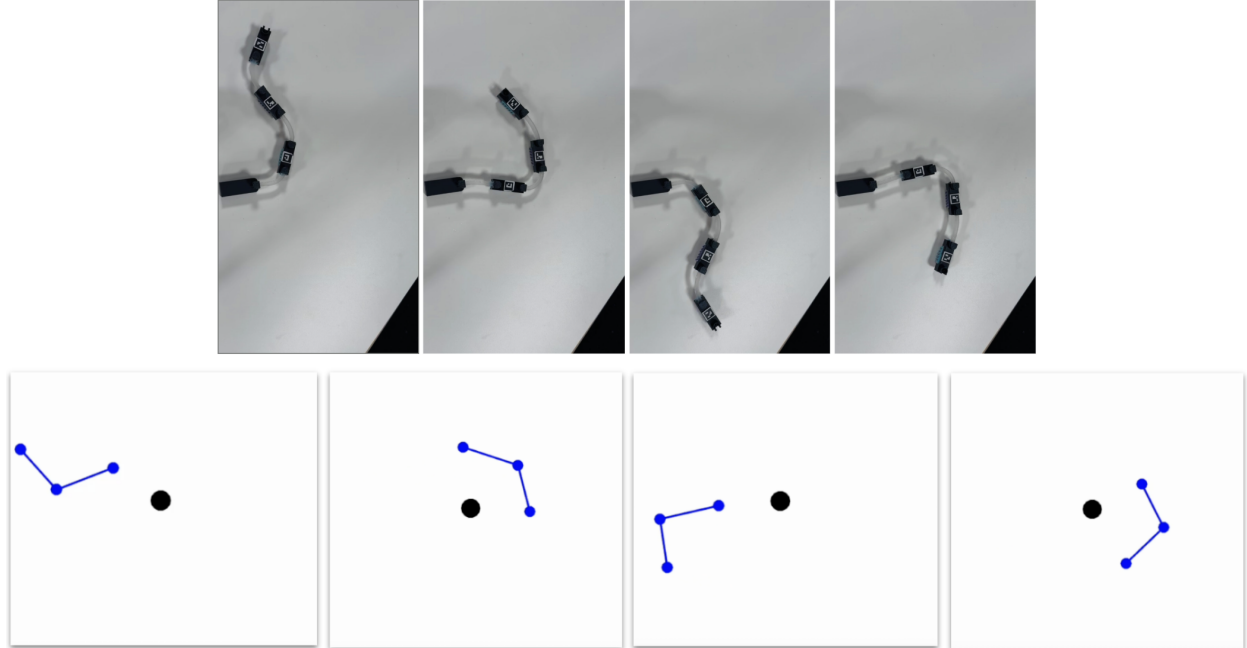


Figure 15: Trial #5 ($N = 3, \sigma = 4.4366$) Experimental reference frames (top row) and Simulation reference frames (bottom row)

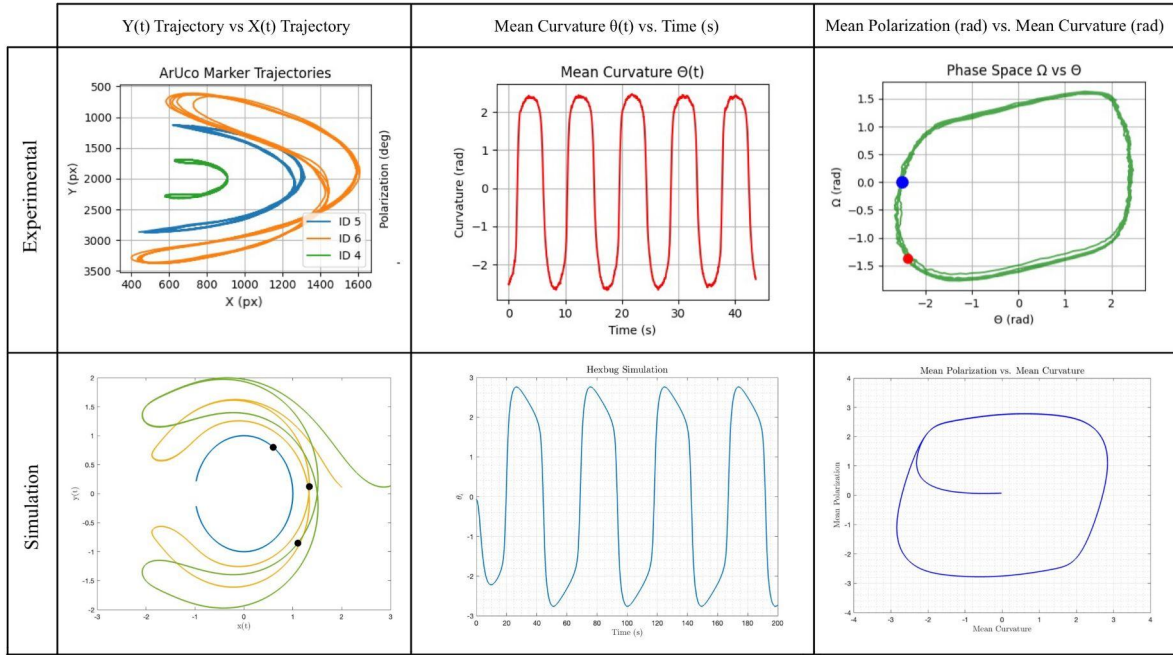


Figure 16: Trial #5 ($N = 3, \sigma = 4.4366$) Tracking data and corresponding graphs (top row) and Simulation generated plots (bottom row)

Multifilament System

Following our experimentation, we began to explore multifilament dynamics through the lens of synchronization. We first began with a fixed base model with 4 ‘prongs’ coming off of the center at 90 degree angles. From there, we attached two $N = 3, \sigma = 4.4366$ filaments attached 180 degrees from one another at opposite sides of the central body (Figure 17). When the Hexbugs were turned on, this yielded a synchronization pattern where the two filaments moved in-phase with one another, mimicking a swimming mode similar to that of a cilium. In addition, we also observed out-of-phase behaviors where the filaments would desync before returning to their original synchronization pattern. Such desynchronization behavior is likely related to the minor differences in each Hexbug’s natural frequency, as well as small geometric differences in the silicone linkages. In turn, these small discrepancies collectively yield brief desynchronizations before the model returns to its in-sync equilibrium.

Following our fixed model, we moved to a rotation model where the position was fixed with free rotation allowed via a central ball bearing with two $N = 3, \sigma = 4.4366$ filaments (Figure 18). With this model, we observed rotation about the point in the clockwise direction, which upon applying an impulse to fix the rotation point, reversed direction to rotate in the counterclockwise direction. Given our initial qualitative observations in response to our multifilament synchronization studies, further research can be done to characterize and visualize the system’s response in light of an applied force.

We then proceeded with our model, adapting our system for four $N = 2, \sigma = 4.4366$ filaments (Figure 19). With this system, we observed 45 degree out-of-phase behavior where the two filaments along the vertical axis and the two filaments along the horizontal axis showed collective behavior. By visual inspection, we found that when the vertical filaments were in transit (wave-like behavior) that the horizontal filaments were at a local maxima and vice versa as the oscillation continued.

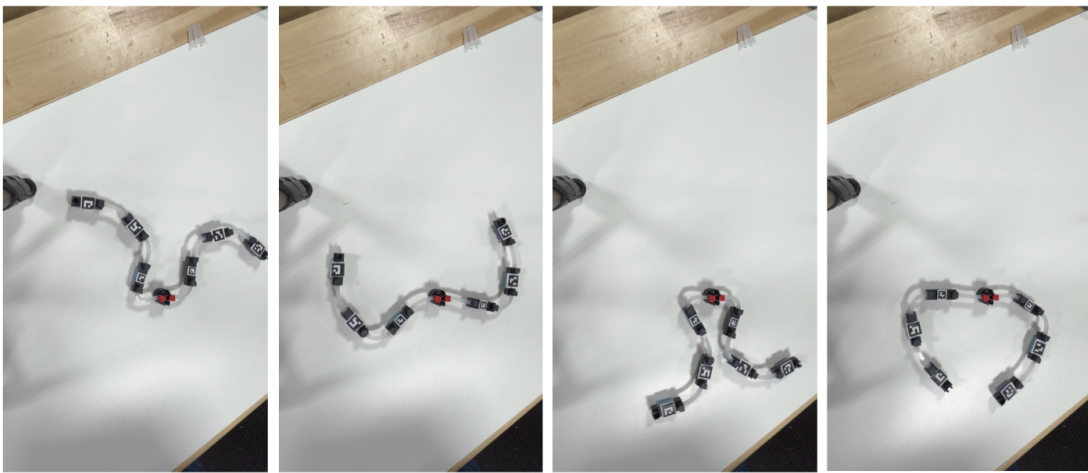


Figure 17: Two $N = 3$, $\sigma = 4.4366$ filament system attached to a fixed center body.

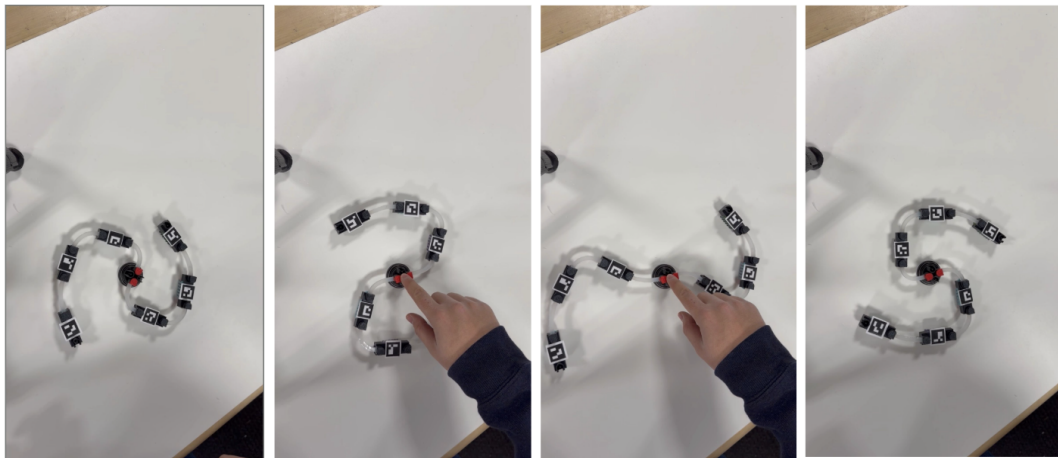


Figure 18: Two $N = 3$, $\sigma = 4.4366$ filament system attached to a rotating center body.

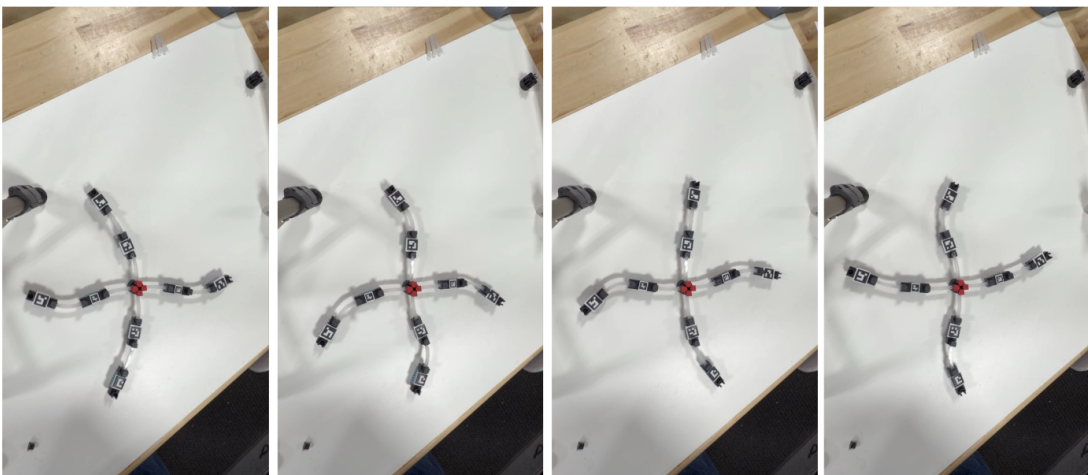


Figure 19: Four $N = 2$, $\sigma = 4.4366$ filament system attached to a fixed center body.

Conclusion

Following the completion of our experimentation, simulations, and subsequent modeling, we found that Hexbug filaments serve as an effective means of modeling and experimentally evaluating elasto-active systems in active matter, dynamic systems. Through our variation of both the linkage and filament length, we were able to establish that the onset of oscillation is both a function of the number of Hexbugs in the filament, N , and the σ , the elasto-activity of the linkage, as predicted by our mathematical model. Filaments with smaller values of σ showed straight-line trajectories with the onset of oscillation taking place somewhere between $\sigma = 1.0071$ and 1.8800 , with higher values of σ producing longer periods of oscillatory behavior.

Comparison between the experimental trajectories and the mathematical model showed relative agreement in the oscillation, mode shape, and phase behavior. Whilst quantitative differences remained between both the model and the experimental observations, likely due to friction and active force contributions, the model successfully captured the physics governing filament behaviors.

Our findings also indicate that synchronization is possible with elasto-active elements through the application of silicone linkages between Hexbugs. Beyond our findings with single-filament behavior, we saw that Hexbug systems can show both synchronization and phase-locking behaviors. With the two and four-filament systems, we observed both synchronous behaviors in and out-of-phase in addition to desynchronization events likely due to asymmetric linkages, small differences in cage placement, and variations in Hexbug natural frequency. As such, this indicates that our model may allow for close comparison with biological cilia and flagella systems, mimicking complex biological behaviors. In addition, the ability to induce swimming-like modes and rotational motion highlights the ability of our model to study gait and locomotion in active matter systems.

Currently, our model is complete and ready for application to further study single-filament and synchronization phenomenon. That being said, additional functionality is entirely possible and is highly recommended to reduce error and enhance both the scope and applications of our model. This includes:

1. Building individual Hexbugs to reduce any ‘drift’ error where the Hexbugs have a general tendency to lean towards the right, both with and without the attached Hexbug cage. Such drift is randomized, with some bugs seeing more significant drift than others due to manufacturing differences. As such, building our own Hexbugs would eliminate this drift.
2. To control for power differences, we could link our individually built Hexbugs to a central power supply and eliminate any differences in supplied power to each component.
3. To reduce issues in the silicone linkages, further work could be done on the encapsulated molds to prevent leakage and ensure the mold is completely full to reduce the error of excess silicone attached to the link. In addition, controlling the curing conditions with time, humidity, and temperature would enhance the accuracy of our results by unifying the material properties across all links.

In regards to our remaining questions as to the future of our experimental model, we pose the following questions in relation to the coding and simulations behind our model:

1. How can we more robustly track the orientation and positioning of our Hexbugs beyond QR code tracking? Is there a way to further minimize any sort of “skipping” when some bugs are enduring lots of rotation in a short amount of time?
2. How can we reduce and/or better account for noise in our modeling?
3. Is there a way for us to test the active force of our particular Hexbugs (commercially or in-house) and would this help our simulation mirror what we are seeing in real-life?

By answering these questions, we hope to refine our model such that our reproducibility might be enhanced and allow us to pose more refined findings that might have significant impact on our understanding of ciliated behaviors. In addition to our questions regarding software, we also would like to better understand and explore the hardware and design setup supporting our experiment and as such wish to answer the following:

1. How can we create a DV-powered homemade model to better simulate collective behavior and brownian motion as opposed to our current model?
2. How can we best implement our design to reduce Hexbug drift and skew towards one direction?
3. How can we best optimize and control cure conditions for the silicone linkages and how might other elastomer linkages impact our model? How do linkage length, stiffness, and cage geometry impact the range and modes of motion in our filament system?
4. How can we elicit multi-filament synchronization in Hexbug behavior? To what extent can we see phase-locking and symmetric movement compared to biological cilia?

If this project were to continue in the future, we would advise the following steps be taken:

1. Revision of the physical model through individual Hexbug design & DV control
 - a. By developing our own DV-powered Hexbug design, we'd get to see its motion unimpacted by commercial manufacturing and thus get to validate our model without taking into account defects in supplier processing. In addition, this would allow us to control the native skew present in commercially available Hexbugs by modifying our own design to reduce any drift effects. In addition, by further controlling the silicone mold curing conditions, we'd be able to enhance the accuracy of our model and ensure reproducibility.
2. Improve our tracking software to track a multifilament system to compare angular motion, mean polarization, and mean curvature
 - a. Currently, our tracking software can only handle calculating the mean polarization and the mean curvature of a one-filament system. Expanding on our project, ideally, we would want to be able to accurately track a multifilament system, correctly identifying and tracking what Hexbugs correlate to what filament and comparing their relative angular motion, mean polarization, and mean curvature.
3. Explore synchrony conditions to analyze how to better induce synchronization and the thresholds for which synchronization might take place.
 - a. Through improving both the tracking and physical model, we would be able to begin enhancing our investigation into synchronization of our multi-filament model of which our findings would prove to be extremely beneficial to the scientific community in exploring how to model active particles to simulate real-world phenomenon.

Appendix

Digital Repository

Found [here](#) and contains our bill of materials, sustainability in engineering initiative, materials flow, all code and CAD, and building and operating instructions.

10R Strategy

In the last leg of our project, we really focused on the refurbishment of our Hexbugs. Hexbugs come with an incredibly high cost and long lead times, causing them to be difficult to acquire. A vital part of our project was comparing our simulations to real-world experiments, and so a lot of time was spent running the Hexbugs, leading to a loss in power and an overall weaker Hexbug. Buying more Hexbugs would have been costly and taken a lot of time, and so to solve our battery problem, we took our Hexbugs apart and replaced their batteries. Not only was this more sustainable, but this also allowed us to have more consistent experiments as we were able to reasonably regulate the battery level in the Hexbug.

Throughout this project as a whole, we focused a lot on reusing and remanufacturing. For the silicone linkages, we reused silicone from an old project of Andrew's. This allowed us not to add extra cost for our project, while extending the utility of this silicone that otherwise would have been discarded. Focusing on repurposing, we achieved this in two ways. We created molds for our silicone linkages and 3-D printed changes that can attach and reattach to different Hexbugs. The molds allow us to create more linkages without creating any more excessive plastic waste. The modularity of the Hexbug cages allows us to reattach the cages to different Hexbugs if our Hexbugs become damaged and unusable in any way. Also, the connectors that we have created in the Hexbugs allow for different silicone linkages (and linkages that fit the given geometry) to attach and detach. The modularity of our design allows for a multitude of iterations of experiments, without producing repetitive parts.

AI Use

- Spring Constant Image Processing and Young's Modulus Calculation: When calculating the Spring constant, we examined the deflection of the beam as we added masses from the bottom of the linkages for all four lengths. Through this process, we collected numerous photos, where we decided on image processing using Matlab to collect the data and find the spring constant for us. We then took that spring constant data and used Matlab to quickly compute the Young's Modulus
 - Prompts used:
 - Create a Matlab script to calculate the spring constant of beams. We have 3 folders, named small, medium, and large, all filled with jpgs that are named the mass in grams. In each of the photos prompt the user to click the beginning and end of the beam, and then in that same photo prompt the user to click 100mm on a ruler to scale for mm/pixel
 - Create a Matlab script to calculate the Young's Modulus given the last code. The cross sectional area is a rectangle.
- Hexbugs ArUco Video Processing: When tracking the position and angle of the Hexbugs we used Python to read and collect the data. We had long 20+ second videos shot at 120 fps, which is long to process and sift through. We utilized ArUco codes to track the Hexbugs as they have directionality and can track position.
 - Prompts used:

- Create a Python script to track objects that have ArUCo trackers on them. We want to track angles and positions. Also, make plots of their X vs Y position and a plot of then make more plots vs time. These plots would be the angles of all of the Hexbugs (to help with debugging), mean polarization (defined as the average value of all angles), mean curvature (the angle of the first bug minus the last bug), and the phase space (defined as mean curvature vs mean polarization).
- Create 16 ArUco codes from 1-16 for us to use in our tracking.
- Hexbug Single Filament Simulation:

Infographic

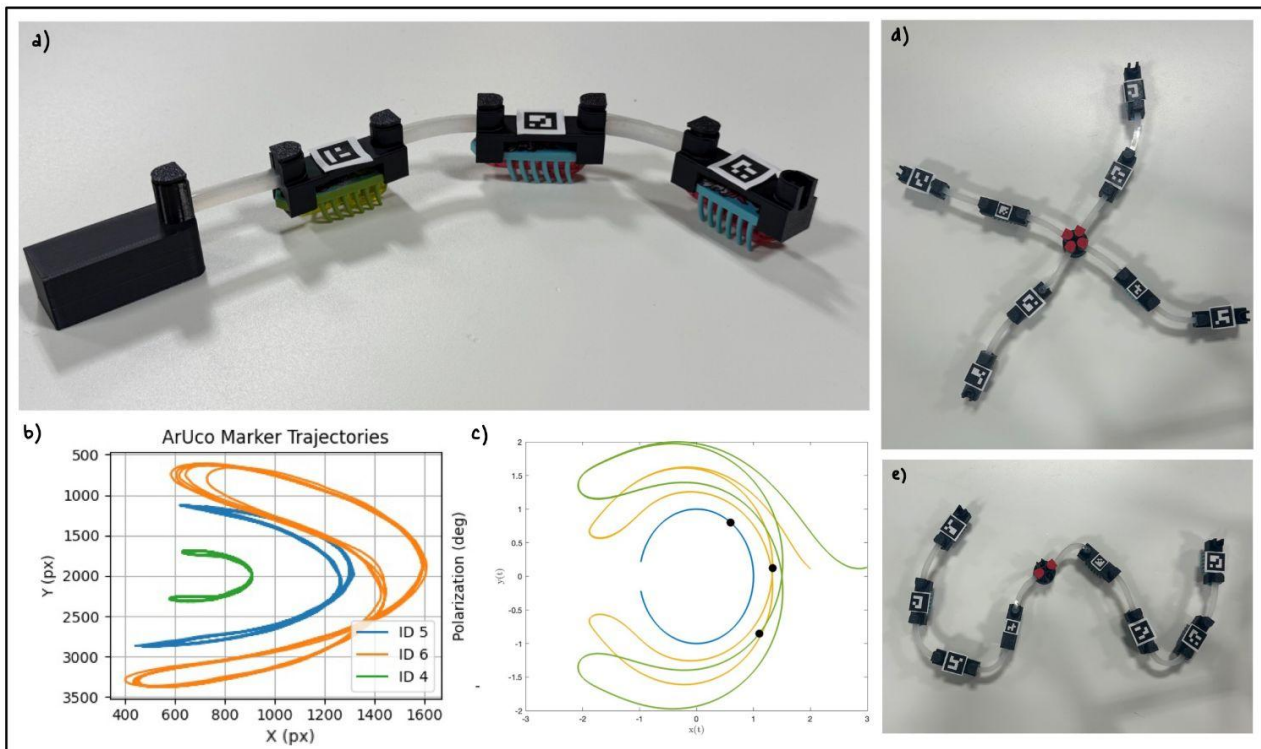


Figure 17: (a) Hexbug Filament, (b) Experimental Trajectory of Hexbug Filament, (c) Simulation Trajectory of Hexbug Filament, (d) Four Filament Hexbug System, (e) Two Filament Hexbug System